Combustion Modeling Study for GCH_4/LOX and GCH_4/GOX Single Element Combustion Chambers

By T. Haga†, D. Muto†, Y. Daimon†, H. Negishi†, T. Shimizu†, AND O. Haidn‡

Japan Aerospace Exploration Agency,
3-1-1, Yoshinodai, Chuo-ku, Sagamihara, Kanagawa, Japan

Single element combustion chambers (GCH_4/LOX and GCH_4/GOX) are numerically investigated. Firstly, the CH_4/LOX single-element combustion chamber simulation was performed by a practical Reynolds-averaged Navier-Stokes solver. A dense gas approach with a cubic equation of state is assessed for the sub-critical condition. The later parts are devoted for developing an efficient wall model for hydrocarbon reacting flows and a high-order algorithm, that will be essential for high fidelity and practical large-eddy simulations. As a benchmarking case, the GCH_4/GOX single-element chamber is considered. The frozen wall model is proposed and $a\ priori$ tests show that it can accurately predict the wall heat flux using a coarse near-wall grid. A high-order unstructured algorithm is developed for turbulent non-premixed combustion using the flamelet approach. To suppress non-physical oscillations across the material interface with variable thermodynamic properties, the so-called enthalpy-based formulation is used.

1. Introduction

Oxygen/methane is an attractive propellant combination in the space propulsion field due to their ease in handling, low operational costs, and high specific impulse. Although the liquid oxygen/methane propellant combination is an attractive option, only a limited amount of experimental data at relevant combustion chamber conditions is available. Improving our knowledge about the heat transfer processes and cooling methods in the combustion chamber is crucial to develop high-performance liquid rocket engines. In this study, single element combustion chambers (GCH_4/LOX and GCH_4/GOX) are numerically investigated. An experimental test campaign is undergoing at the Technical University of Munich (TUM) on a gaseous methane (GCH_4)/liquid oxygen (LOX) shear coaxial single element injector. In Section 2, the corresponding Reynolds-averaged Navier-Stokes (RANS) simulations are performed and the results are compared with the experimental data. Proper numerical modeling on the equation-of-state, the surface tension, and so on is important depending on the experimental conditions.

The later parts of this report are devoted for developing the numerical modeling and algorithm that are essential for the practical Large-eddy Simulation (LES). Although LES is believed to be able to improve prediction accuracy over RANS, its computational cost is a critical issue, especially for assessing wall heat transfer. To validate the developed

† Research and Development Directorate, Japan Aerospace Exploration Agency
‡ Department of Mechanical Engineering, Technical University of Munich

code, the GCH_4/GOX single-element chamber is considered, which was investigated experimentally and numerically in the prior Summer Programs. In Section 3, a novel wall stress model accounting for the reacting flow is proposed to alleviate the intense computational cost of LES. In Section 4, a scalable high-order unstructured algorithm on many core systems is employed to further improve the computational efficiency.

2. CH_4/LOX single element combustion chamber simulations

2.1. *Motivation*

In the past two summer program, the benchmarks for GCH_4/GO_2 single- [11] and multi-element [12] combustion chamber have been carried out using CRUNCH CFD [8]. The simulation code and modeling have been validated using the pressure profiles, heat flux distributions, and wall temperature. The simulation results showed good agreement with the experimental data.

This framework evolved from GCH_4/GO_2 to GCH_4/LOX combustion simulation. Therefore, the effect of non-ideal gas will be evaluated by the benchmark simulation of GCH_4/LOX single-element combustion chamber. As a first step to evaluate the non-ideal gas effect, the so-called dense gas approach was selected even though the combustion pressure was lower than the critical one.

2.2. *Computational setup*

The numerical simulations in this study were conducted using the density-based solver CRUNCH CFD [8], which is an unstructured/multi-element flow solver based on a cell vertex method [8,9]. The general computational methods were basically the same as the past reports [10–12]. The governing equations were the three-dimensional compressible Reynolds-averaged Navier-Stokes equations. Inviscid fluxes were calculated using a second-order linear reconstruction procedure based on a total variable diminishing scheme. Viscous fluxes were computed by estimating gradients at cell faces. The standard high Reynolds number $k-\epsilon$ turbulence model was used. The near-wall treatment within the $k-\epsilon$ model were based on the two layer model [13]. For time integration, an implicit solution procedure was employed, allowing for Gauss-Seidel or generalized minimal residual over options with a preconditioning matrix using a distance-one neighbor bandwidth [9]. For the combustion model, laminar finite rate model with a skeletal chemical reaction set of CH_4/O_2 proposed by DLR [7] was used. This model includes 21 species and 97 chemical reactions. The thermodynamic properties and the transport properties were calculated for each chemical species. Those properties of the mixture gas were then evaluated based on fundamental mixing rules. The thermodynamic properties of oxygen was computed by a cubic equation of state, the Soave-Redlich-Kwong equation [14]. For the other chemical species including H_2O, the ideal gas assumption was applied. The viscosity and thermal conductivity of oxygen were given by Ely and Hanley formulation based on the corresponding state principle [15, 16].

Figure 1 shows the computational domain, which is a half of CH_4/LOX thrust chamber. For boundary conditions, the supersonic outflow condition is imposed on the nozzle outlet, and the mass flow rates and static temperatures of CH_4 and LOX are specified at inlet boundaries for each fluid, as shown in Table 1, and thus, the chamber pressure obtained by the computation can be compared with the experimental data. A non-slip and isothermal wall with 500 K.

The number of computational grid points is approximately 7 million, in which the y^+

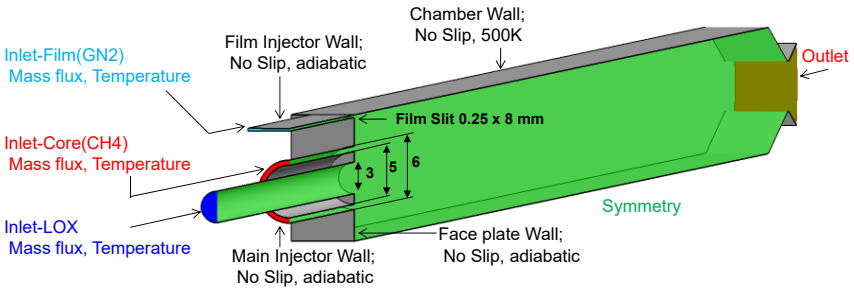

FIGURE 1. Computational domain and boundary conditions

TABLE 1. Inlet conditions

O/F		3.06
LOX mass flow rate	g/s	46.1
LOX temperature	K	96.8
GCH_4 mass flow rate	g/s	15.0
GCH_4 temperature	K	268
N_2 mass flow rate	g/s	3.16
N_2 temperature	K	293

of the near-wall grid is about 0.1 along the entire region and a hexahedra mesh with 20 grid points is used on the LOX post. The grid system is sufficient downstream of the LOX post has been changed from prism to hexahedra at the middle of chamber.

2.3. *Validations relative to experimental data*

Figure 2 shows a comparison of wall pressure profiles on the chamber wall between the experimental data and simulation results. The experimental data shows a steep drop from 0 to 100 mm in the combustion chamber. After 150 mm in the combustion chamber, the pressure profile of experimental data shows a gradual decrease. The simulation pressure shows the steeper drop from 0 to 100 mm than the experimental data. In addition, the pressure level was 1 – 2 % higher than the experimental data. As a result, the simulation results suggest that the combustion in the simulation has completed faster than in the experiment. The ignoring of an atomization and vaporization process in this simulation yielded the fast combustion progress.

Figure 3 shows temperature and mass fraction distributions of CH_4, O_2, and N_2. The high temperature region, which corresponds to the diffusion flame, extends gradually. The low temperature region at the corner in combustion chamber corresponds to high concentration region of CH_4 and N_2. The mass fraction of CH_4 near the N_2 slot was relatively lower than that of the bottom corner. The mass fraction of O_2 was not symmetry in the vertical direction because of the N_2 injection. In the latter half of the combustion chamber, temperature distribution was almost constant. CH_4 mass fraction distribution vanished at the border of diffusion flame very clearly due to the chemical reaction. On the other hand, N_2 mass fraction distribution vanished in downstream gradually due to

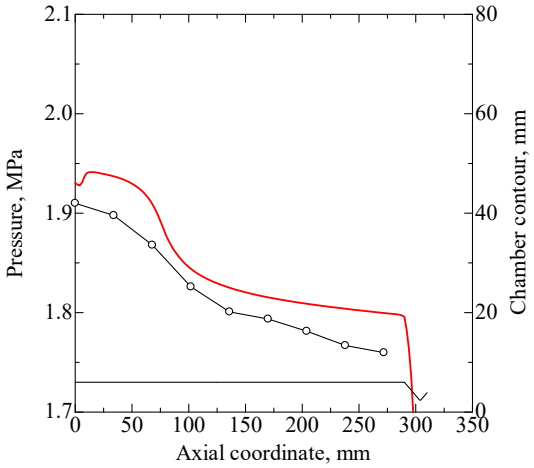

FIGURE 2. Wall pressure profiles in thrust chamber

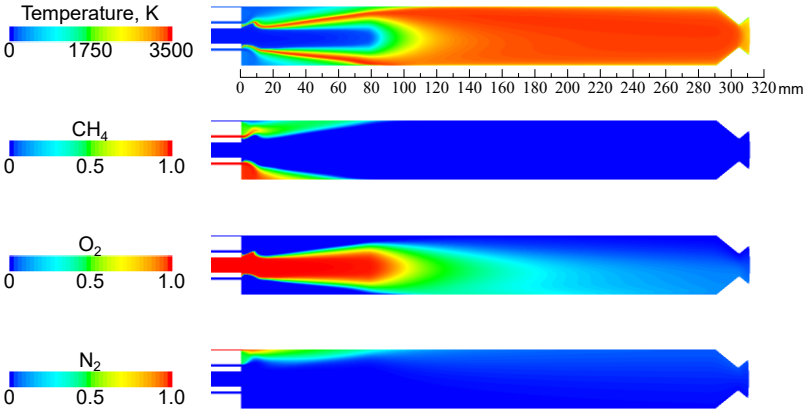

FIGURE 3. Temperature and mass fraction contours for Methane, Oxygen, and Nitrogen

the diffusion in the combustion chamber. We could clearly understand the difference between the reaction of CH_4 and diffusion of N_2.

3. Wall modeling for CH_4/O_2 reacting flows

3.1. *Motivation*

An accurate prediction of the wall heat flux in combustion chambers using LES still remains a challenging problem. This is because of the huge computational cost for resolving the turbulent boundary layer. The viscous length scale at the chamber wall approaches $O(1\ \mu\mathrm{m})$, and resolving the viscous length scale significantly increases the number of cells of the computational grid and decreases the time step. One approach to overcoming this difficulty is a wall-modeled LES (WMLES), which has been successfully demonstrated its validity for aerodynamic problems. The idea behind WMLES is resolving the outer layer while modeling the inner layer, as the inner layer model is used to estimate wall shear stress and heat flux. When applying WMLES to combustion cham-

bers, an inner layer model is needed that considers near-wall thermal and chemical effects. Near the chamber wall, a significant temperature change from the burnt gas to the cooled wall results in changes in thermodynamic gas properties. Additionally, the heat loss at the wall can cause chemical reactions and subsequent changes in the chemical composition within the boundary layer.

Towards applying WMLES to CH_4/O_2 combustion chambers and accurately predicting the wall heat flux, this study proposes an inner layer model that is valid for hydrocarbon reacting flows. The study performs $a\ priori$ tests with comparing existing inner layer models. This study uses the ordinary-differential-equation (ODE) based wall models assuming equilibrium and frozen chemistry [1, 2], the standard wall function [3], and the coupled wall function [4].

3.2. *Formulation*

One ODE-based wall model is the equilibrium wall model developed by Muto et al. [1]. With the boundary-layer approximation and the chemical equilibrium assumption, the boundary layer equations for velocity and temperature are obtained as follows:

$$\frac{d}{dy}\left[(\mu+\mu_t)\frac{dU_{||}}{dy}\right]=0, \tag{3.1}$$

$$\frac{d}{dy}\left[\left(\lambda+\frac{c_p\mu_t}{Pr_t}+\frac{\mu}{Sc}\sum_{k=1}^{N}h_k\left.\frac{dY_k}{dT}\right|_{\text{eq.}}+\frac{\mu_t}{Sc_t}\sum_{k=1}^{N}\Delta h^o_{f,k}\left.\frac{dY_k}{dT}\right|_{\text{eq.}}\right)\frac{dT}{dy}\right] + \frac{d}{dy}\left[(\mu+\mu_t)U_{||}\frac{dU_{||}}{dy}\right]=0. \tag{3.2}$$

where $U_{||}$ is the wall parallel velocity, μ is the viscosity, T is the temperature, λ is the thermal conductivity, c_p is the specific heat at constant pressure. h_k, Y_k, and $\Delta h^o_{f,k}$ are the enthalpy, mass fraction, and the chemical enthalpy of formation of species k, respectively. μ_t, Pr_t, and Sc_t are the eddy viscosity and the turbulent Prandtl and Schmidt number, respectively. The inner-layer eddy viscosity is modeled by using the mixing length model [5]:

$$\mu_t=\kappa\rho\sqrt{\frac{\tau_w}{\rho}}y[1-\exp(-y^\star/A^+)]^2, \tag{3.3}$$

where τ_w is the wall shear stress, and κ=0.41 and A^+ = 17 are model constants. Here, $y^*=\rho u^*_\tau y/\mu$ and $u^*_\tau=\sqrt{\tau_w/\rho}$ known as the semi-local properties are used instead of the classical wall units of $y^+=\rho_w u_\tau y/\mu_w$ and $u_\tau=\sqrt{\tau_w/\rho_w}$.

The coupled ODEs of Eqs. (3.1) and (3.2) with the mixing length model of Eq. (3.3) are numerically solved by using a one-dimensional finite volume method. The values of chemical terms and gas properties at a chemical equilibrium corresponding to given temperature, pressure, and initial chemical composition are pre-tabulated using a chemical equilibrium calculation. This wall model was successfully validated in H_2/O_2 reacting flows [1].

Another ODE-based wall model is the frozen wall model assuming the frozen chemistry [1,2]. This wall model solves following equation for temperature instead of Eq. (3.2):

$$\frac{d}{dy}\left[\left(\lambda+\frac{c_p\mu_t}{Pr_t}\right)\frac{dT}{dy}\right]+\frac{d}{dy}\left[(\mu+\mu_t)U_{||}\frac{dU_{||}}{dy}\right]=0. \tag{3.4}$$

The gas properties are calculated with a constant mixture composition with respect to the temperature and pressure in the wall model.

Both ODE-based wall models applies $Sc = Pr$ with assuming the Lewis number is unity, where $Pr = \mu c_p/\lambda$ is the Prandtl number. Detailed descriptions of the ODE-based wall models can be found in Muto et al. [1].

In addition to the ODE-based wall models, two wall function models are also tested. One is the model by Spalding and Launder [3], which assumes constant properties and single component flows. Another is the coupled wall function by Cabrit and Nicoud [4], where the both wall shear stress and heat flux are function of the velocity, temperature, and chemical composition.

3.3. *Turbulent reacting channel flows*

The test case is LES of the reacting turbulent channel flow conducted by Cabirt and Nicoud [4]. The working fluid used in the simulation is a mixture containing seven species of H_2, H, H_2O, OH, CO_2, CO, and N_2, which is a typical combination of many industrial combustors. The temperatures of the mixture and the wall are 3150 K and 1050 K, respectively. The free stream Mach number is 0.2, and the friction Reynolds number is 1000. In the ODE-based wall models and the standard wall function, model constants of Pr_t and Sc_t are set to 0.9. The coupled wall function uses Pr_t and Sc_t of 0.7, which were proposed values by Cabirt and Nicoud [4]. The LES solutions at different wall normal locations are applied as the boundary condition of the models.

Figure 4 shows the wall shear stress and heat flux predicted by the different models. The calculated wall shear stress and heat flux are normalized by the LES results. The results show that the ODE-based wall models are superior to the wall functions: the two wall functions show large discrepancies in both wall shear stress and heat flux. In a comparison between the equilibrium and frozen wall models, while both models show an almost the same wall shear stress, the frozen wall model provides a more accurate in predicting the wall heat flux.

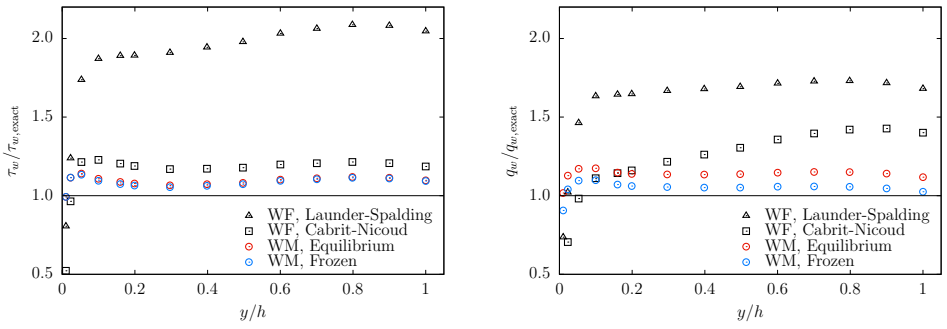

(a) Wall shear stress (b) Wall heat flux

FIGURE 4. Comparison of wall shear stress and heat flux in wall models in the reacting turbulent channel flow. $\tau_{w,exact}$ and $q_{w,exact}$ are the wall shear stress and heat flux of the LES results [4].

Figure 5 compares chemical compositions predicted by the equilibrium and frozen wall models. The LES results [4] are also plotted. While the LES observes small changes in the chemical composition according to chemical reactions due to heat loss, the chemical composition is almost constant near the wall. The wall model that assumes frozen chemistry well predicts the LES results. In contrast, the equilibrium wall model shows

discrepancies from the LES results because the changes in chemical compositions are overpredicted. This indicates that the chemical reactions do not reach equilibrium near the wall and thus the chemical frozen assumption is reasonable for hydrocarbon reacting flows.

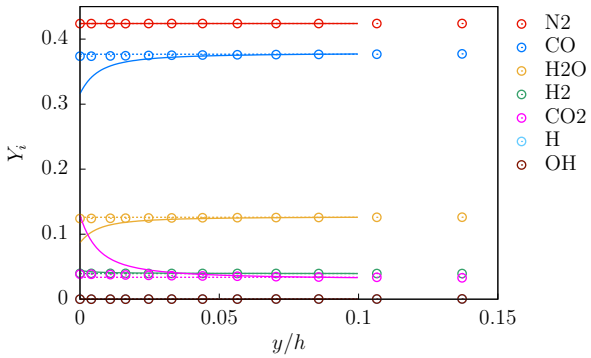

FIGURE 5. Chemical compositions and temperature in the reacting channel flow. Circles, LES results [4]; lines, the equilibrium wall model; dashed lines, the frozen wall model.

Consequently, it is expected that the frozen wall model can be used as an inner layer model for hydrocarbon reacting flows.

3.4. *GCH_4/GOX rocket combustion chamber*

Here, the frozen wall model is coupled with a Reynolds-Averaged Navier Stokes (RANS) simulation, which will be referred as WMRANS. The test case is a GCH_4/GOX single-element rocket combustor firing test conducted at the Technical University of Munich [6]. The oxidizer to fuel ratio is 2.64, and the target chamber pressure is 1.88 MPa. The inlet temperatures of CH_4 and O_2 are 269 K and 275 K, respectively.

The RANS is performed by using JAXA's in-house CFD solver LS-FLOW, which is an arbitrary polyhedral unstructured compressible flow solver that solves the three-dimensional compressible Navier-Stoke equations for conserved variables of mass, momentum, and total energy. The equations are closed with the ideal gas equation of state. The standard $k-\epsilon$ turbulence model and the finite rate chemistry with a skeletal reaction mechanism [7] are solved. The one-dimensional wall model grid is embedded in the RANS domain, which is 0.2 mm thick and has 41 grid points. At the top boundary of the wall model, a set of RANS solutions of wall-parallel velocity, temperature, pressure, and chemical compositions is applied. Non-slip and iso thermal conditions are applied at the bottom boundary. After the wall-model is solved, the obtained wall shear stress and wall heat flux are fed back to the RANS as wall boundary conditions. The wall-normal grid spacing is $20\ \mu\mathrm{m}$ corresponding to $y^+ \sim 40$. In addition to WMRANS, this study performs RANS with a grid resolving the wall with the wall-normal grid spacing of $0.1\ \mu\mathrm{m}$ corresponding to $y^+ \sim 0.2$.

Figure 6 shows wall heat flux profiles along the chamber wall as well as the measured results [6]. Both WMRANS and RANS accurately predict the wall heat flux overall. Note that the wall-normal grid width of WMRANS is 200 times that of RANS. WMRANS predicts the wall heat flux with reasonable accuracy even with such a coarse near-wall grid.

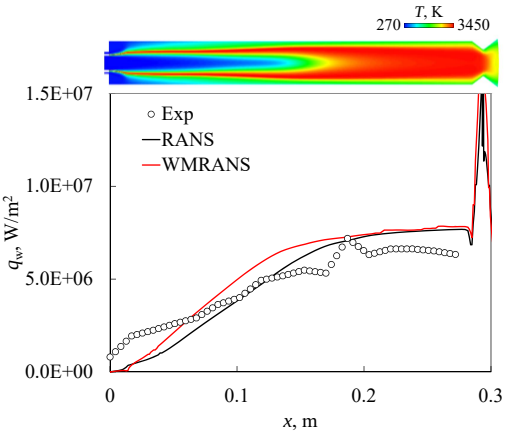

FIGURE 6. Wall heat flux profiles in the GCH_4/GOX rocket combustion chamber. The temperature contour of WMRANS is also shown.

A comparison between WMRANS and RANS, however, shows that WMRANS predicts a higher wall heat flux around x =0.03 to 0.2 m. This region corresponds to that the boundary layer is developing, suggesting that the effects of model parameters need to be assessed in the developing boundary layer such as the length of the wall model grid that corresponds to the thickness of the modeled inner layer.

Applying the frozen wall model to WMLES and its validation is the subject of future work.

4. Development of a high-order unstructured LES solver

4.1. *Motivation*

High-order methods can drastically reduce the number of grid points i.e. the computational cost on scale resolving simulation such as LES and DNS. However, most of the conventional CFD solvers are based on a second-order algorithm when complex geometries for practical applications are considered. For LES modeling, there is another concern that large numerical dissipation caused by such low-order algorithms often interferes with modeling performance. Recently the discontinuous finite element methods (DFEM) such as the Discontinuous Galerkin (DG) or Flux Reconstruction (FR) [18] methods have gained attention due to their arbitrary high-order of accuracy on unstructured grids and excellent parallel performance on recent many core systems. A high-order compressible FR solver for reacting flow is under development in JAXA based on the success for high Reynolds number LES of supersonic jets [19]. In this study, a flamelet-based combustion model is employed for the LES of the GCH_4/GO_2 single element chamber [17].

4.2. *High-order method and formulation*

Thermodynamic properties in multicomponent flows are not constant but depend on temperature and species composition. Abgrall and Karni [21] showed that differences in the specific heat ratio across the material interface induce spurious pressure oscillations if a fully conservative scheme is used. This problem is more serious with high-order methods that have much less numerical dissipation. There are several approaches to

suppress non-physical oscillations. Karni [20] first solved the pressure evolution equation in stead of solving the total energy. Terashima and Koshi [22] extended this approach to the transcritical flow. Another simple and successful approach is the double flux method [21].

In this study, the enthalpy-based (HB) approach by Lacaze et al. [23] is employed. The conventional fully conservative governing equations read:

$$\frac{\partial \rho}{\partial t} + \nabla \cdot (\rho \boldsymbol{u}) = 0, \tag{4.1}$$

$$\frac{\partial \rho \boldsymbol{u}}{\partial t} + \nabla \cdot (\rho \boldsymbol{u} \otimes \boldsymbol{u} + P\underline{\boldsymbol{\delta}} - \underline{\boldsymbol{\tau}}) = 0, \tag{4.2}$$

$$\frac{\partial \rho e_t}{\partial t} + \nabla \cdot [\rho e_t \boldsymbol{u} + (P\underline{\boldsymbol{\delta}} - \underline{\boldsymbol{\tau}})\,\boldsymbol{u} + \boldsymbol{q}_e] = 0, \tag{4.3}$$

where ρ is the density, $\boldsymbol{u}$ is the velocity vector, P is the static pressure, $\underline{\boldsymbol{\delta}}$ is the unit tensor, $\underline{\boldsymbol{\tau}}$ is the viscous stress tensor, e_t is the total energy per unit mass and $\boldsymbol{q}_e$ is the energy diffusion flux. In addition to the above system, the HB approach solves the pressure evolution equation to transport the total enthalpy $(h_t = e_t + P/\rho)$.

$$\begin{aligned}\frac{\partial P}{\partial t} + \nabla \cdot (P\boldsymbol{u}) = &- \left(\rho c^2 - P\right) \nabla \cdot \boldsymbol{u} - \frac{c^2 \rho_T}{\rho C_p} \left(\underline{\boldsymbol{\tau}} : \underline{\boldsymbol{S}} - \nabla \cdot \boldsymbol{q}_e\right) \\ &+ \sum_{k=1}^{N_s} \frac{c^2}{\rho C_p} \left(\rho_T h_{Y_k} - \rho_{Y_k} C_p\right) \left(-\nabla \cdot \boldsymbol{q}_k\right),\end{aligned} \tag{4.4}$$

where c is the speed of sound, C_p is the heat capacity at constant pressure, $\boldsymbol{q}_k$ is the mass diffusion flux and $\underline{\boldsymbol{S}}$ is the strain rate tensor. In this study, the ideal gas law is used and the derivatives of ρ and h are analytically evaluated. The transport properties are calculated by a power-law function, and the heat capacity is calculated by the NASA polynomials. Note that the sub-grid scale terms are omitted and implicit LES is performed by using an upwind flux scheme at the cell interfaces.

The chemical reaction is modeled by the steady flamelet approach. The transport equation for the mixture fraction Z is given as:

$$\frac{\partial \rho Z}{\partial t} + \nabla \cdot (\rho \boldsymbol{u} Z - \rho D_Z \nabla Z) = 0, \tag{4.5}$$

where D_Z is the diffusion coefficient assuming the unity Lewis number. The HB approach can maintain the interface equilibriums, however, spurious oscillations can occur at steep gradient of density. A localized artificial diffusivity approach for multicomponent flows by Terashima et al. [22] is used to robustly capture interface discontinuities. For the spatial discretization, the FR method with hexahedral cells is used. The solution points to store the degrees-of-freedom (DOFs) within each cell are chosen to be the Gauss points. At the cell interfaces where the solution can be discontinuous, the SLAU scheme and the Bassi and Rebay 2 (BR2) scheme are used for the inviscid and viscous fluxes, respectively. For the time integration, the third-order TVD Runge-Kutta scheme is used. In order to verify the developed code, one-dimensional material advection and diffusion problems were considered. If the material interface is sufficiently smooth, the solution obtained with the HB approach was confirmed to be almost the same as with the fully conservative approach.

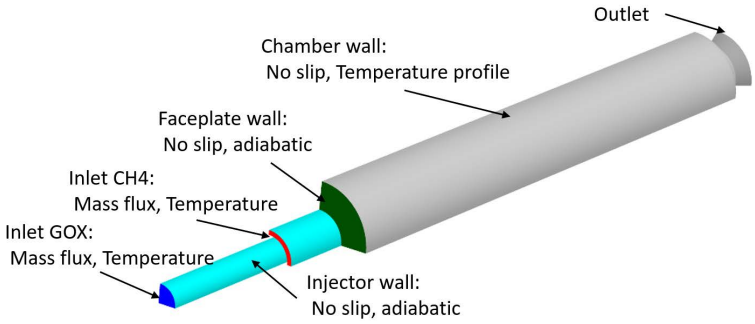

FIGURE 7. Computational domain and boundary conditions.

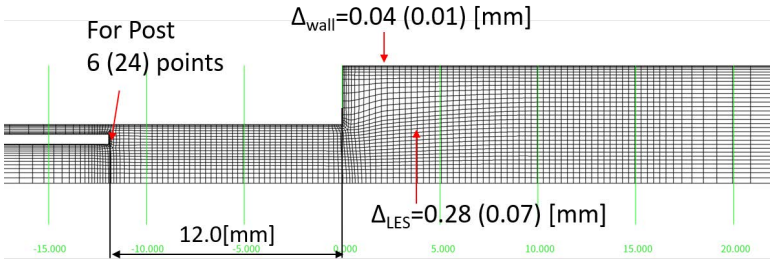

FIGURE 8. Computational mesh.

4.3. *LES of the CH_4/GOX single-element combustion chamber*

The single element GCH_4/GOX shear coaxial combustion chamber, which was used in the static firing tests conducted by Silvestri et al. [17], is considered. Figure 7 shows a computational domain with the boundary conditions. The 1/4 domain of the circular cylinder chamber is modeled to reduce the computational cost, and the symmetric boundary condition is assumed on the symmetric cross section. The oxidizer to fuel ratio is 2.2, and the target chamber pressure is 20 bar. Here, the recess length is set to 12 mm. The inlet and wall boundary conditions are the same as the RANS simulation by Daimon et al. [11].

The computational mesh near the injector is shown in Fig. 8. The total cell number is only 104,016 but the total solution points are 2.8 millions and 6.6 millions for P2 and P3 computations, respectively. Note that The numbers in parentheses are the target resolution with P3 (4th-order) computation. A preliminary computation was conducted by the FR P2 (3rd order) scheme. The computed flowfield is shown in Fig. 9. Although quantitative comparison with the experiment is needed, the unsteady flow feature can be captured even with the small number of DOFs.

The developed code has not been tuned yet, but it takes about 12 hours for 500,000 steps ($\sim$ 1 ms) using 36 nodes (1152 cores) of the Fujitsu FX100 system. Further computations to obtain a statistically converged solution are underway, and comparative studies with different recess lengths will be reported in the future.

5. Conclusions

In this study, single element combustion chambers (GCH_4/LOX and GCH_4/GOX) are numerically investigated using various turbulence modeling approaches.

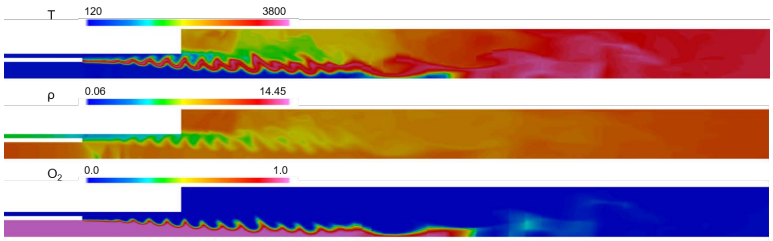

FIGURE 9. Instantaneous flowfield.

Firstly, the CH_4/LOX single-element combustion chamber simulation was performed by RANS. The computed wall pressure profile indicates the faster combustion progress due to the dense gas approach used in this study. In near future, the computed wall heat flux distribution will be compared with the experimental data.

Secondly, a novel wall model for hydrocarbon reacting flows is proposed and assessed by $a\ priori$ tests. A comparison of existing inner layer models demonstrated that the ODE-based wall model based on frozen chemistry is superior to that based on equilibrium chemistry and the wall function models in the reacting channel flow case. For the GCH_4/GOX single-element chamber, wall-modeled RANS with the frozen wall model can accurately predict the wall heat flux on a much coarse near-wall grid resolution, compared to conventional RANS.

Finally, a high-order unstructured algorithm is developed for turbulent non-premixed combustion using the flamelet approach. So far, only preliminary results have been obtained, but highly efficient computation on many core systems can be expected. The combination of the wall model and the high order solver will be the building block to achieve the high fidelity LES of full scale combustors.

Acknowledgments

Financial support has been provided by the German Research Foundation (Deutsche Forschungsgemeinschaft – DFG) in the framework of the Sonderforschungsbereich Transregio 40. Computational resources have been provided by the JAXA Supercomputer System Generation 2 (JSS2).

References

[1] MUTO, D., DAIMON, Y., SHIMIZU, T. AND NEGISHI, H. (2019). An equilibrium wall model for reacting turbulent flows with heat transfer. *International Journal of Heat and Mass Transfer*, **141**, 1187–1195. DOI 10.1016/j.ijheatmasstransfer.2019.05.101.

[2] KAWAI, S. AND LARSSON, J. (2012). Wall-modeling in large eddy simulation: Length scales, grid resolution, and accuracy. *Physics of Fluids*, **24**, 015105. DOI 10.1063/1.3678331.

[3] LAUNDER, B.E. AND SPALDING, D.B. (1974). The numerical computation of turbulent flows. *Computer Methods in Applied Mechanics and Engineering*, **3**, 269–289.

[4] CABRIT, O. AND NICOUD, F. (2009). Direct simulations for wall modeling of multicomponent reacting compressible turbulent flows. *Physics of Fluids*, **21**, 055108. ISSN 10706631. DOI 10.1063/1.3123528.

[5] YANG, X.I. AND LV, Y. (2018). A semi-locally scaled eddy viscosity formulation for LES wall models and flows at high speeds. *Theoretical and Computational Fluid Dynamics*, **32**, 617–627. DOI 10.1007/s00162-018-0471-3.

[6] ROTH, C., SILVESTRI, S., PERAKIS, N. AND HAIDN, O. (2017). Experimental and numerical investigation of flow and combustion in a single element rocket combustor using GH2 / GOX and GCH4 / GOX as propellants. In: *31st International Symposium on Space Technology and Science (ISTS)*. 2017-o-4-01.

[7] SLAVINSKAYA, N.A., ABBASI, M., WEINSCHENK, M. AND HAIDN, O.J. (2015). Methane skeletal mechanism for space propulsion applications. *5th International Workshop on Model Reduction in Reacting Flows*.

[8] HOSANGADI, A., LEE, R.A., YORK, B.J., SINHA, N. AND DASH, S.M. (1996). Upwind Unstructured Scheme for Three-Dimensional Combustion Flows. *Journal of Propulsion and Power*, **12**, 494–503. DOI 10.2514/3.24062.

[9] HOSANGADI, A., LEE, R.A., CAVALLO, P.A., SINHA, N. AND YORK, B.J. (1998). Hybrid, Viscous, Unstructured Mesh Solver for Propulsive Applications. In: *34th AIAA/ASME/SAE/ASEE Joint Propulsion Conference and Exhibit*. AIAA1998-3153. DOI 10.2514/6.1998-3153.

[10] CHEMNITZ, A., SATTELMAYER, T., ROTH, C., HAIDN, O., DAIMON, Y., KELLER, R., GERLINGER, P., ZIPS, J. AND PFITZNER, M. (2017). Numerical Investigation of Reacting Flow in a Methane Rocket Combustor: Turbulence Modeling. *Journal of Propulsion and Power*, **34**, 864–877. DOI 10.2514/1.B36565.

[11] DAIMON, Y., TERASHIMA, H., NEGISHI, H., CELANO, M.P., SILVESTRI, S. AND HAIDN, O. (2016). Combustion Modeling Study for GCH4/GOX single element combustion chamber: Steady State Simulation and Validations. In: *Space Propulsion Conference 2016*. SP2016-3125263.

[12] DAIMON, Y., NEGISHI, H., SILVESTRI, S. AND HAIDN, O. (2018). Conjugated Combustion and Heat Transfer Simulation for a 7 element GOX/GCH4 Rocket Combustor. In: *2018 Joint Propulsion Conference*. AIAA2018-4553. DOI 10.2514/6.2018-4553.

[13] WOLFSHTEIN, M. (1969). The Velocity and Temperature Distribution in One-dimensional Flow with Turbulence Augmentation and Pressure Gradient. *International Journal of Heat and Mass Transfer*, **12**, 301–318. DOI 10.1016/0017-9310(69)90012-X.

[14] SOAVE, G. (1972). Equilibrium constants from a modified Redlich-Kwong equation of state. *Chemical Engineering Science*, **27**, 1197–1203. DOI 10.1016/0009-2509(72)80096-4.

[15] ELY, J.F. AND HANLEY, H.J.M. (1981). Prediction of transport properties. 1. Viscosity of fluids and mixtures. *Ind. Eng. Chem. Fundamen.*, **20**, 323–332. DOI 10.1021/i100004a004.

[16] ELY, J.F. AND HANLEY, H.J.M. (1983). Prediction of transport properties. 2. Thermal conductivity of pure fluids and mixtures. *Ind. Eng. Chem. Fundamen.*, **22**, 90–97. DOI 10.1021/i100009a016.

[17] SILVESTRI, S., CELANO, M.P., SCHLIEBEN, G., KNAB, O. AND HAIDN, O. (2016). Experimental Investigation on Recess Variation of a Shear Coax Injector in a GOX-GCH4 Combustion Chamber. In: *Space Propulsion Conference 2016*. SP2016-3124836.

[18] HUYNH, H.T. (2007). A flux reconstruction approach to high-order schemes including discontinuous Galerkin methods. In: *18th AIAA Computational Fluid Dy-*

namics Conference. AIAA2007-4079. DOI 10.2514/6.2007-4079.

[19] HAGA, T. AND KAWAI, S. (2019). On a robust and accurate localized artificial diffusivity scheme for the high-order flux-reconstruction method. *Journal of Computational Physics*, **376**, 534 – 563. DOI 10.1016/j.jcp.2018.09.052.

[20] KARNI, S. (1994). Multicomponent flow calculations by a consistent primitive algorithm. *Journal of Computational Physics*, **112**, 31 – 43. DOI 10.1006/jcph.1994.1080.

[21] ABGRALL, R. AND KARNI, S. (2001). Computations of compressible multifluids. *Journal of Computational Physics*, **169**, 594 – 623. DOI 10.1006/jcph.2000.6685.

[22] TERASHIMA, H. AND KOSHI, M. (2012). Approach for simulating gas-liquid-like flows under supercritical pressures using a high-order central differencing scheme. *Journal of Computational Physics*, **231**, 6907 – 6923. DOI 10.1016/j.jcp.2012.06.021.

[23] LACAZE, G., SCHMITT, T., RUIZ, A. AND OEFELEIN, J.C. (2019). Comparison of energy-, pressure- and enthalpy-based approaches for modeling supercritical flows. *Computers & Fluids*, **181**, 35 – 56. DOI 10.1016/j.compfluid.2019.01.002.